Magnetic Eye Tracking: A New Approach Employing a Planar Transmitter

Anton Plotkin, Oren Shafrir, Eugene Paperno*, and Daniel M. Kaplan

***Abstract*—A new scleral search coil (SSC) tracking approach employing a planar transmitter has been developed theoretically and tested experimentally. A thin and flat transmitter is much more convenient in installation, operation, and maintenance than the conventional large cubic one. A planar transmitter also increases the mobility of SSC systems, simplifies their accommodation in a limited clinical space, enables bedside testing, and causes no visual distractions and no discomfort to the users. Moreover, it allows tracking not only the SSC orientation, but also its location, which is very important for many medical and scientific applications. The suggested approach provides the speed and precision that are required in SSC applications. The experimental results show that it can be used for the diagnosis of vestibular disorders. The tracking precision is in good agreement with its theoretical estimation.**

***Index Terms*—Eye tracking, planar transmitter, scleral search coil (SSC).**

I. Introduction

TRACKING the human eye is an important topic in modern life sciences, psychology, and medicine. It allows, for example, the diagnosis of neurologic, ophthalmologic, and vestibular disorders [1]–[6]. In such diagnosises, very fast saccadic eye movements should be measured with very high precision.

Conventional scleral search coil (SSC) systems comprise a large cubic transmitter [see Fig. 1(a)]. Their principle of operation is quite straightforward. The cubic transmitter generates three magnetic fields that are nearly orthogonal and homogenous in its operating volume. Each field induces in the SSC a voltage that is proportional to the cosine of the angle between the SSC axis and the field direction. The three SSC voltages provide enough information for calculating the two SSC orientation angles (azimuth and elevation) with reference to the cubic transmitter.

Fig. 1. Magnetic tracking of the human eye. (a) Conventional system employing a cubic transmitter. (b) New system employing a planar transmitter.

An important advantage of the large cubic transmitter is that its wide area of the transmitting coils easily provides the required strength of the magnetic fields, and thus, a high SNR and a high-tracking precision. Another important advantage of the cubic transmitter is that the SSC orientation can be found by using very simple analytical relations. As a result, a high-tracking speed can be achieved with a relatively low-computational power.

On the other hand, the principal disadvantage of the large cubic transmitter is its bulkiness and awkwardness, causing difficulties in installation, operation, and maintenance. The cubic transmitter may also cause visual distractions and discomfort to the users. Another principle disadvantage of the cubic transmitter is due to the systematic tracking errors caused by the unavoidable inhomogeneity of its magnetic fields. For example, the systematic errors are as large as 1% even for a transmitter that is threefold greater than its operating volume [7].

In this paper, we suggest a new SSC tracking approach employing a planar transmitter [see Fig. 1(b)]. A thin and flat transmitter is much more convenient in installation, operation, and maintenance. Employing a planar transmitter reduces both the total volume occupied by the tracking system and its constructional complexity. A planar transmitter also increases the mobility of SSC systems, simplifies their accommodation in a

Manuscript received June 24, 2009; revised September 21, 2009 and November 27, 2009. First published February 17, 2010; current version published April 21, 2010. This work was supported in part by the Analog Devices, Inc., in part by the National Instruments, Inc., and in part by the Ivanier Center for Robotics Research and Production Management, Ben-Gurion University, Beer-Sheva, Israel. *Asterisk indicates corresponding author.*

A. Plotkin is with the Department of Electrical and Computer Engineering, Ben-Gurion University of the Negev, Beer-Sheva 84105, Israel and also with the Department of Neurobiology, Weizmann Institute of Sciences, Rehovot 76100, Israel (e-mail: antonp@ee.bgu.ac.il; shafrir@ee.bgu.ac.il).

O. Shafrir is with the Department of Electrical and Computer Engineering, Ben-Gurion University of the Negev, Beer-Sheva 84105, Israel (e-mail: shafrir@ee.bgu.ac.il).

*E. Paperno is with the Department of Electrical and Computer Engineering, Ben-Gurion University of the Negev, Beer-Sheva 84105, Israel (e-mail: paperno@ee.bgu.ac.il).

D. M. Kaplan is with the Department of Otolaryngolgy-Head and Neck Surgery, Soroka University Medical Center, Faculty of Health Sciences, Ben-Gurion University of the Negev, Beer-Sheva 84105, Israel (e-mail: dankap@bgu.ac.il).

Color versions of one or more of the figures in this paper are available online at http://ieeexplore.ieee.org.

Digital Object Identifier 10.1109/TBME.2009.2038495

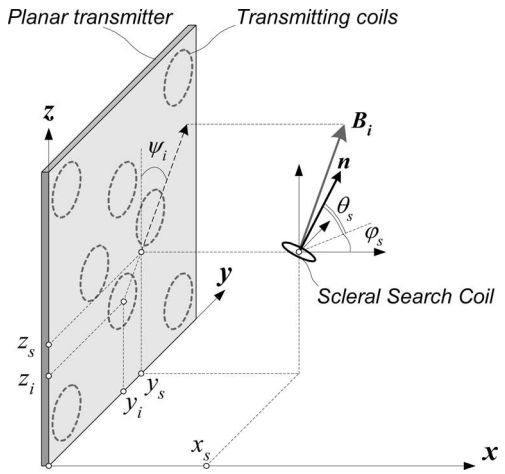

Fig. 2. Scleral search coil in the coordinate system of the planar transmitter.

limited clinical space, enables bedside testing, and causes no visual distractions and no discomfort to the users. Moreover, it allows tracking not only the SSC orientation, but also its location, which is very important for many medical and scientific applications.

II. Method

A. Transmitter Configuration

To most efficiently utilize the transmitter volume for generating as strong as possible magnetic fields, we employ a coplanar array of transmitting coils (see Fig. 2). This allows us to keep the transmitter thin. Employing noncoplanar transmitting coils would significantly increase the transmitter thickness and make it rather bulky.

To keep the whole system simple, we employ the minimum possible number of transmitting coils arranged in a special pattern (see Fig. 2). Our numerical simulations have shown that the minimum number of coplanar transmitting coils, providing the continuous tracking of a search coil, is eight. We have also found that the pattern of eight coplanar coils, as shown in Fig. 2, provides the best tracking precision for a given operating volume.

We excite each transmitting coil at its own frequency with a sine-wave current. The gap between the frequencies is chosen large enough to avoid the overlapping of the sidebands of the adjacent frequencies. This allows us to excite all the transmitting coils continuously and simultaneously. A sequential excitation at one and the same frequency, while reducing the occupied frequency span, would decrease the tracking accuracy due to the longer delays between the successive measurements of the SSC voltage.

To eliminate the crosstalk caused by mutual magnetic couplings between the transmitting coils [8], we apply a new method that, in contrast to [8], does not require any additional hardware, we simply measure, and then, consider the crosstalk components in the described later tracking algorithm.

B. Tracking Algorithm

To find the five DOF of the SSC $(x_s, y_s, z_s, \theta_s, \varphi_s)$ (see Fig. 2), we solve the following system of eight nonlinear equations:

$$\mathbf{v} = \mathbf{SCBn} \tag{1}$$

where $\mathbf{v} = [V_1, V_2, \ldots. V_8]^T$ is the vector of the voltage amplitudes at the SSC output (the index denotes the transmitting coil number and its operating frequency, and the upper-case T denotes vector transposition)

$$\mathbf{S} = \begin{bmatrix} S_1 & 0 & \cdots & 0 \\ 0 & S_2 & \cdots & 0 \\ \vdots & \vdots & \ddots & \vdots \\ 0 & 0 & \cdots & S_8 \end{bmatrix} \tag{2}$$

is the matrix of the SSC sensitivities at different frequencies

$$\mathbf{C} = \begin{bmatrix} 1 & C_{12} & \cdots & C_{18} \\ C_{21} & 1 & \cdots & C_{28} \\ \vdots & \vdots & \ddots & \vdots \\ C_{81} & C_{81} & \cdots & 1 \end{bmatrix} \tag{3}$$

is the matrix of crosstalk coefficients. Each row in (3) shows the ratios of the crosstalk components and the excitation current in a transmitting coil

$$\mathbf{B} = \begin{bmatrix} B_{x1} & B_{y1} & B_{z1} \\ B_{x2} & B_{y2} & B_{z2} \\ \vdots & \vdots & \vdots \\ B_{x8} & B_{y8} & B_{z8} \end{bmatrix} \tag{4}$$

is the matrix of the magnetic field components at the SSC location (x_s, y_s, z_s). The components $(B_{x_i}, B_{y_i}, B_{z_i})$ are given as follows [9]:

$$\begin{aligned} B_{x_i} &= \frac{I_i \mu_0}{2\pi R} \frac{1}{\sqrt{Q_i}} \left[E(k_i) \frac{1 - \alpha_i^2 - \beta_i^2}{Q_i - 4\alpha_i} + K(k_i) \right] \\ B_{y_i} &= \sin\psi_i \frac{I_i \mu_0}{2\pi R} \frac{\gamma_i}{\sqrt{Q_i}} \left[E(k_i) \frac{1 + \alpha_i^2 + \beta_i^2}{Q_i - 4\alpha_i} - K(k_i) \right] \\ B_{z_i} &= \cos\psi_i \frac{I_i \mu_0}{2\pi R} \frac{\gamma_i}{\sqrt{Q_i}} \left[E(k_i) \frac{1 + \alpha_i^2 + \beta_i^2}{Q_i - 4\alpha_i} - K(k_i) \right] \\ k_i &= \sqrt{\frac{4\alpha_i}{Q_i}} \\ \alpha_i &= \frac{\sqrt{(y - y_i)^2 + (z - z_i)^2}}{R} \\ \beta_i &= \frac{x - x_i}{R} \\ \gamma_i &= \frac{x_i}{\sqrt{(y - y_i)^2 + (z - z_i)^2}} \\ Q_i &= (1 + \alpha_i)^2 + \beta_i^2 \end{aligned} \tag{5}$$

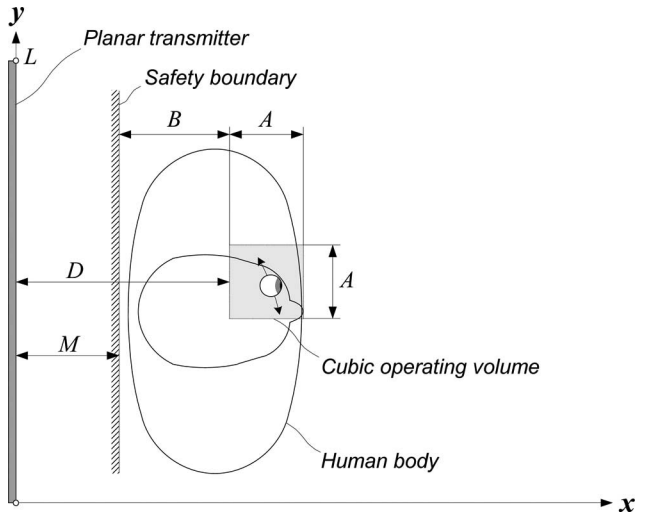

Fig. 3. Operating volume for measuring the gain of the VOR. In this example, the scleral search coil is attached to the left eye.

where $i = 1,\ldots,8$ denotes the transmitting coil number $\psi_i = \arctan[(y - y_i)/(z - z_i)]$ is the angle between the z-axis and the projection of the magnetic field on the yz-plane (see Fig. 2), (x_i, y_i, z_i) is the location of the transmitting coil, I_i is the excitation current amplitude, R is the transmitting coil radius, μ_0 is the permeability of free space, $K(k_i)$ and $E(k_i)$ are the complete elliptic integrals of the first and second kinds.

$$\mathbf{n} = [\cos\varphi_s \cos\theta_s, \sin\varphi_s \cos\theta_s, \sin\theta_s]^T \tag{6}$$

in (1) is the vector describing the SSC orientation.

To solve (1), we use the Levenberg–Marquardt algorithm [10], which provides both reliable and fast convergence.

C. Random Errors

In this section, we estimate the worst random errors that are caused by the SSC output noise, which is mainly due to the electronic noise of the preamplifier (the SSC thermal noise is negligible). Processing the noisy SSC output yields erroneous measurements of both the SSC location and orientation. We define the random location errors σ_r, as the rms of the difference between the measured and the true SSC locations. Similarly, we define the random orientation errors λ_r, as the rms of the difference between the measured and the true SSC orientations.

For a given noise level and excitation current in the transmitting coils, the worst random errors all over the entire operating volume, σ_R and λ_R are a function of the system geometrical dimensions. We assume that the size of the operating volume is constant $A = 10$ cm (see Fig. 3). Thus, the worst random errors are a function of the transmitter size L, the distance between the transmitter and the operating volume D, the radius of the transmitting coils R, and the radius r_s, and the number of turns n_s, of the SSC.

To find the worst random errors σ_R and λ_R, for given L, D, R, r_s, and n_s, we have applied the differential evolution algorithm [11]. At each step of the algorithm, a population of 64 SSC positions was generated according to the best-exponential strategy. The random location and orientation errors, where obtained for each SSC position by loading 10^3 realizations of noisy SSC outputs into the tracking algorithm. In all the calculations, the SSC output noise was set at 21 $\mathrm{nV_{rms}}$ that corresponds to a 1.5 nV/Hz noise of the SSC preamplifier multiplied by the square root of the 200-Hz operating bandwidth. The SSC output voltage was calculated using the parameters of a typical SSC: $r_s = 9$ mm, $n_s = 7$, and a 10 kHz excitation frequency.

In the earlier simulations, the excitation current in the transmitting coils was adjusted based on the following considerations. To provide as small as possible random errors, the excitation current and the tracking fields should be as strong as possible. On the other hand, the tracking field magnitudes should comply with safety standards [12], defining the maximum level of magnetic fields acting on the human body. Therefore, for each distance between the transmitter and the operating volume D, we have chosen such excitation current that the maximum safe level of the tracking fields $B_{\max} = 0.1$ mT, is attained at the safety boundary (see Fig. 3) that is located at a distance $B = 15$ cm from the operating volume. This distance is large enough to avoid the action of unsafe tracking fields on the human body. The maximum distance between the transmitter and the safety boundary M, is defined by the maximum available power dissipation and the voltage drop across the transmitting coils. These limitations depend on the size of the transmitting coils. We have calculated M for transmitting coils of two representative radii: $R = 5$ and 10 cm. For $R = 5$ cm, we have obtained $M = 14$ cm, and for $R = 10$ cm, we have obtained $M = 15.7$ cm.

The results of our calculations have shown that for each radius of the transmitting coils R, there exists an optimum distance D^* between the operating volume and the transmitter that minimizes the worst random errors σ_R and λ_R for any transmitter size L. For $R = 5$ cm, this distance $D^* = 29$ cm, and for $R = 10$ cm, $D^* = 31$ cm.

Considering the earlier values of D^*, we have summarized our results in Fig. 4, where the worst random errors σ_R and λ_R are shown as a function of the transmitter size L, and the radius of the transmitting coils R is a parameter. The worst random errors at the center of the operating volume are shown by the dashed lines.

It can be seen from Fig. 4 that for $R = 5$ cm, the worst random orientation errors reach minima at $L = 65$ cm. For the same $L = 65$ cm, choosing $R = 10$ cm reduces both σ_R and λ_R by 20%. However, for $R = 10$ cm, decreasing the transmitter size below $L = 60$ cm causes overlapping of the transmitting coils. To have flexibility in building our experimental setups, we have used transmitting coils with an $R = 5$ cm radius, inspite of the fact that this causes somewhat higher random errors.

D. Systematic Errors

In this section, we find the systematic errors that are caused by the inhomogeneity of the magnetic tracking fields seen by the SSC and compare them against the random errors found in the previous section. The SSC output voltage (1) is proportional to the average magnetic field penetrating the SSC area [9]. It has been assumed in (1)–(6) that the SSC radius is negligible

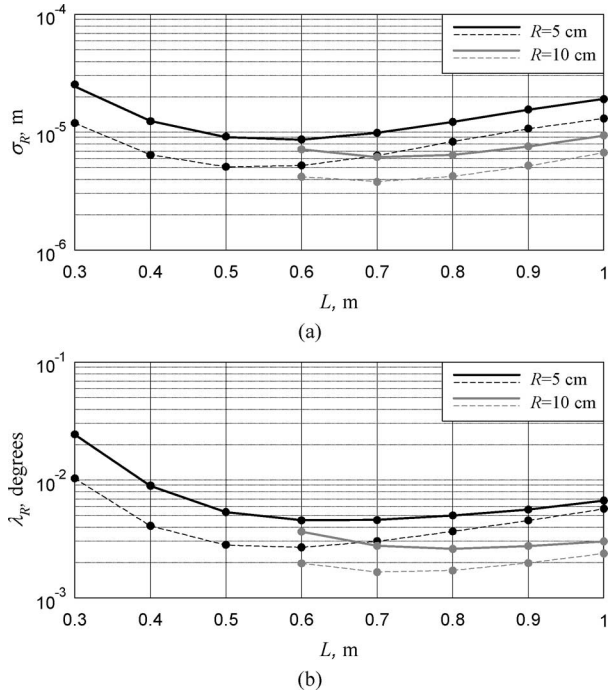

Fig. 4. Worst random location errors σ_R, in (a) and worst random orientation λ_R, in (b) errors as a function of the transmitter size L (see Fig. 3), for the given size of the operating volume $A = 10$ cm. The errors at the center of the operating volume are shown by the dashed lines. The radius of the transmitting coils R, is a parameter.

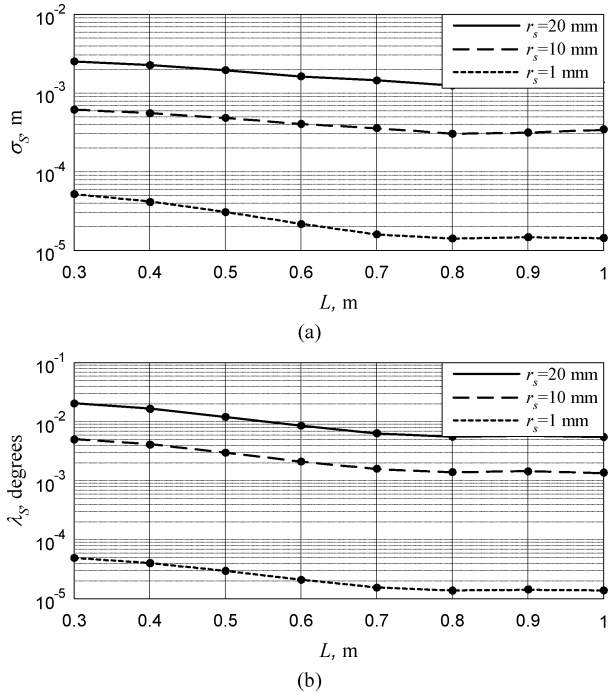

Fig. 5. Worst systematic errors as a function of the transmitter size L (see Fig. 3), for given size of the transmitting coils $R = 5$ cm, and given size of the operating volume $A = 10$ cm. The SSC radius r_s is the parameter. (a) Worst systematic location errors σ_S. (b) Worst systematic orientation errors λ_S.

compared to the distance between the SSC and the transmitter, and the tracking fields across the SSC area are nearly homogenous. In this case, the average magnetic field penetrating the SSC area equals the magnetic field at the SSC center (5). However, the radius of a practical SSC is relatively large, and the average magnetic field differs from the magnetic field at the SSC center. Thus, processing the measured SSC output by the tracking algorithm causes a difference between the measured and the true positions of the SSC. We refer to this difference as the systematic error, which include the systematic location error σ_s, and the systematic orientation error λ_s.

To compare the systematic and the random errors, we have calculated the worst systematic errors all over the entire operating volume σ_S and λ_S, as a function of the transmitter size L, for the following set of the geometrical dimensions (see Fig. 3): the size of the operating volume $A = 10$ cm, the optimum distance between the transmitter and the operating volume $D^* = 29$ cm, the radius of the transmitting coils $R = 5$ cm, and for three different SSC radii r_s. We have employed the same differential evolution algorithm [11] as for the calculation of the worst random errors. The measured SSC output was modeled by averaging the magnetic fields over a number of small SSC subareas, for which the tracking fields are nearly homogenous.

The results of our calculations are shown in Fig. 5. It can be seen from Fig. 5 that for the optimum transmitter size $L = 65$ cm, which minimizes the worst random errors σ_R and λ_R, the worst systematic errors σ_S and λ_S, are also close to their minima. For $L = 65$ cm and $r_s = 10$ mm, the worst systematic location error is $\sigma_S = 0.37$ mm, and the worst systematic orientation error is $\lambda_S = 1.9$ millidegrees. Using these results and the results of Fig. 4, we conclude that for $L = 65$ cm and $r_s = 10$ mm, the accuracy of tracking the SSC location is limited by the worst systematic error $\sigma_S = 0.37$ mm, whereas the accuracy of tracking the SSC orientation is limited by the worst random error $\lambda_R = 4.4$ millidegrees. For a larger SSC, with $r_s = 20$ mm, the tracking accuracy is limited by the systematic errors.

III. Experiment

A. Transmitter Excitation

We have connected each transmitting coil via a capacitor C_i, to a half-bridge excitation circuit (see Fig. 6). The input MOSFET BS170 translates the 5-V digital input into 12-V pulses accepted by the gate driver IR2111 (made by International Rectifiers, Inc.) that drives the gates of two power-MOSFETs IRF540 N. The two 20 Ω resistors limit the MOSFETs gate currents. The 0.1 Ω resistor having 10 ppm/K temperature coefficient is connected in series to the transmitting coil to measure the excitation current.

The capacitance C_i is chosen such that the resonant frequency of the resulting series *LCR* circuit matches the ith excitation frequency. The transmitting coils are excited at the resonant frequencies of 6.25, 8.3, 10, 12.5, 14.3, 16.7, 20, and 25 kHz. The excitation voltages have rectangular waveforms. Due to the relatively high-quality factor of the resonant circuits, the excitation currents approach sinusoidal waveforms. The excitation current amplitudes are 2 A.

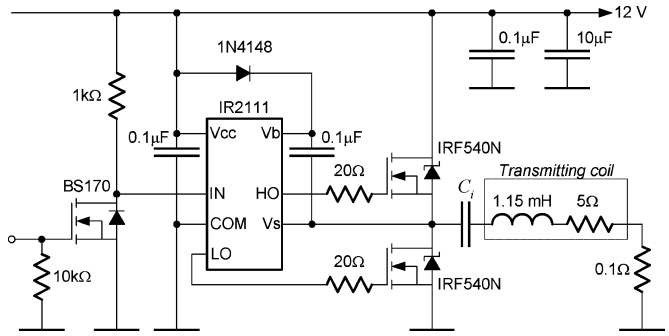

Fig. 6. Half-bridge circuit for the excitation of a single transmitting coil.

B. Receiving Coils

To track the eye position, we have employed a standard SSC (made by Skalar Medical BV). The SSC radius is 9 mm and the number of turns is seven.

To track the head position, we have used a custom-made coil having a 5-mm radius and wound with 200 turns of 60-μm copper wire. This design provides an order of degree higher SNR compared to the SSC. The head coil is mounted on a 5 cm $\times$ 5 cm $\times$ 0.8 cm mouthpiece made of balsa wood. During the experiment, the mouthpiece is gripped by the teeth, which provides reliable tracking of the head position.

Both the SSC and the head coil are connected to low-noise instrumentation amplifiers INA103 A (made by Texas Instruments, Inc.).

C. Data Acquisition and Processing

The data acquisition and processing is done in real time using a modular instrumentation system (made by National Instruments, Inc.). The instrumentation system is composed of an NI PXI 1042B chassis, NI PXI 8186 controller, NI PXI 6533 digital input/output module, and two NI PXI 4272 analog input modules.

The functions of each module are as follows. The digital input/output module controls the transmitter excitation circuits. This module outputs eight digital signals at the excitation frequencies. Each digital signal is the input to the corresponding half-bridge circuit (see Fig. 6). One of the analog input modules samples the outputs of both the SSC and the head coil, and the other analog input module samples the excitation currents. The sample rate of the analog input modules is 100 kS/s. The PXI controller detects the amplitudes of the sampled analog signals and executes the tracking algorithm.

The sampled analog signals are synchronously detected at the eight excitation frequencies and processed according to the tracking algorithm. The detectors comprise fourth-order low-pass Butterworth filters. The bandwidth of each filter is 200 Hz. The excitation currents are used as the reference for the synchronous detection of the outputs of both the SSC and head coil.

D. Experimental Results

To prove experimentally the applicability of the new approach to eye tracking, we have measured the gain of vestibular-ocular reflex (VOR) of two volunteers. One of the volunteers is healthy, and the other volunteer suffers from bilateral Meniere's disease, long-standing on the left ear, and a more recent and severe involvement of the right ear. This disease affects the inner ear and causes a deficit of the peripheral vestibular system.

To calculate the VOR gain of the volunteers, we have measured the position of their eyes and head while applying the active head thrust test [3]. The volunteer under the test is asked to stare at a point in front of him while a medically skilled assistant suddenly and quickly rotates the volunteer's head by a 20–30° angle to the left and to the right. At each head rotation, the instantaneous eye velocity corresponding to the peak head velocity is chosen and their ratio is calculated. The VOR gain is calculated as the average of these ratios, separately for the left-side and the right-side rotations. In our experiments, the point in front of the volunteers' eyes was at a 4 m distance. The head peak velocities were in the range from 150 to 500 degrees/s. The rotations order and occurrence during the test were arbitrary.

The VOR gain of the healthy volunteer was 0.96 for the left-side rotations and 1.02 for the right-side rotations. These gains are very close to the ideal gain of one. Typical time plots of the eye and head azimuths, and the corresponding angle velocities are shown in Fig. 7(a). The diagram of the eye peak velocities versus head peak velocities is shown in Fig. 8(a).

The VOR gain of the volunteer suffering from bilateral Meniere's disease was 0.58 for the left-side rotations and 0.21 for the right-side rotations. Typical time plots of the eye and head azimuths, and the corresponding angle velocities are shown in Fig. 7(b). The graph of the eye peak velocities versus head peak velocities is shown in Fig. 8(b). These results demonstrate that the presence and the degree of the vestibular disorder in this volunteer can be clearly identified.

During the experiment, the typical random orientation errors were 3 millidegrees rms and the typical random location errors were 6 μm rms. These errors are in good agreement with their upper bounds that were found theoretically (see Fig. 4): the worst random orientation error $\lambda_R = 4.4$ millidegrees and the worst random location error $\sigma_R = 9$ μm. To calculate λ_R and σ_R, we have estimated the true locations and orientations as the mean ones.

IV. Discussion

Employing a planar transmitter instead of the cubic one causes the following principal limitations. The first limitation is related to the rapid decrease of the tracking fields with distance. As a result, the SNR and the random tracking errors increase with distance from the transmitter. The second limitation is related to the employment of inherently slower numerical algorithms instead of analytical ones. Thus, a greater computational power is required to obtain the same update rate.

Considering the earlier limitations, it was important for us to examine the suitability of a planar transmitter for eye tracking. To reach this goal, we have analyzed, both theoretically and experimentally, the tracking precision and speed. We have found the *worst* random and systematic tracking errors for a given operating volume as a function of the transmitter size. Our results

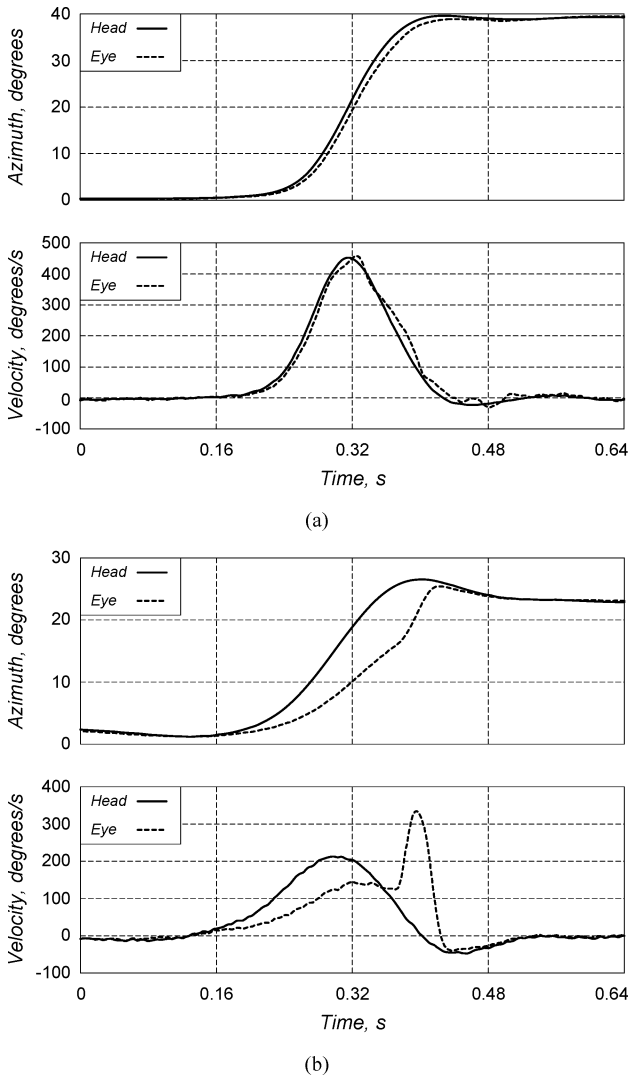

Fig. 7. Typical tracking waveforms. (a) Healthy volunteer. (b) Volunteer with deficit of the peripheral vestibular system.

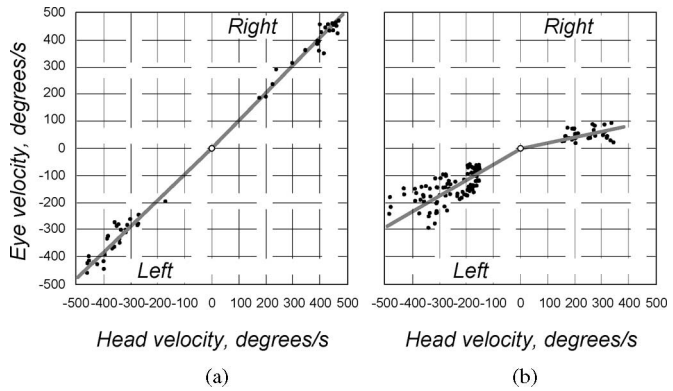

Fig. 8. Diagrams illustrating the calculation of the VOR gain. (a) Normal vestibular system. The right VOR gain is 1.02, the left gain is 0.96. (b) Vestibular system with disease. The right VOR gain is 0.21, the left gain is 0.58.

in Fig. 4 show that there is an optimal transmitter size $L = 0.65$, for which the random tracking errors are as small as 4.4 millidegrees rms and 9 μm rms for transmitting coils with a 5 cm radius. (The typical experimental values of the random tracking errors are 3 millidegrees rms and 6 μm rms.) Fig. 5 shows 1.9 millidegrees and 370 μm systematic errors for the same transmitter and a 1 cm radius of the SSC. The worst tracking accuracy, therefore, is about 15 millidegrees and 0.4 mm, assuming that the random tracking errors are distributed normally and their crest factor is three. To reach the highest tracking speed, we operate the transmitting coils simultaneously and use a special algorithm to eliminate the crosstalk. This provides us with a 650-Hz update rate while running the numerical tracking algorithm on a 2.6-GHz personal computer. The obtained accuracy and speed are comparable with those provided by tracking systems with cubic transmitters [4]: 3.5 millidegrees rms random error, 400 millidegrees systematic error, and up to 2 kHz update rate.

One can see, therefore, that the performance of tracking with a planar transmitter can approach that of a cubic transmitter. We have also demonstrated the effectiveness of the planar transmitter in a practical application, where a VOR gain was measured. Our measurements show (see Fig. 8) that our system is accurate and fast enough to clearly distinguish between the VOR gains of normal and deficient vestibular systems.

Continuing the comparison between the new and conventional systems, we should note that the new system requires more transmitting coils, more operating frequencies, and more excitation hardware. However, the new system is much more compact, rigid, and convenient in operation and maintenance. Moreover, it also provides the tracking of location, not only orientation. In those applications where location monitoring is important, the conventional eye tracking system needs an additional location tracker.

V. Conclusion

A new approach to the SSC tracking employing a planar transmitter has been developed theoretically and tested experimentally. A thin and flat planar transmitter is used instead of the bulky conventional cubic transmitter. The suggested approach provides the speed and precision that are required in SSC applications. The experimental results show that it can be used for the diagnosis of vestibular disorders: typical random orientation errors are 3 millidegrees rms, and typical random location errors are 6 μm rms. These errors are in good agreement with their upper bounds that have been found theoretically $\lambda_R = 4.4$ millidegrees and $\sigma_R = 9$ μm correspondingly.

The result obtained in this paper for tracking precision can be further improved by increasing the radius of the transmitting coils and increasing the excitation frequencies. Noise matching [13] of the SSC preamplifier would also improve the tracking precision.

Suggested in this paper, new crosstalk compensation allows employing simple half-bridge excitation circuits instead of the conventional closed-loop drivers [8]. This improves the power efficiency and simplifies the system hardware.

REFERENCES

[1] A. Oeltermann, S.-P. Ku, and N. K. Logothetis, "A novel functional magnetic resonance imaging compatible search-coil eye-tracking system," *Magn. Reson. Imag.*, vol. 25, no. 6, pp. 913–922, Jul. 2007.

[2] M. M. J. Houben, J. Goumans, and J. V. D. Steen, "Recording three-dimensional eye movements: scleral search coils versus video oculography," *Invest. Ophthalmol. Visual Sci.*, vol. 47, no. 1, pp. 179–187, Jan. 2006.

[3] R. A. Black, G. M. Halmagyi, M. J. Thurtell, M. J. Todd, and I. S. Curthoys, "The active head-impulse test in unilateral peripheral estibulopathy," *Arch. Neurol.*, vol. 62, pp. 290–293, Feb. 2005.

[4] Angle-Meter NT. (2009, Nov. 27). Scleral search coil system for linear detection of three-dimensional angular movements, Primelec, D. Florin, Regensdorf, Switzerland. [Online]. Available: http://www.primelec.ch/datasheets/amnt_datasheet.pdf

[5] F. Vitu, D. Lancelin, A. Jean, and F. Farioli, "Influence of foveal distractors on saccadic eye movements: a dead zone for the global effect," *Vis. Res.*, vol. 46, pp. 4684–4708, 2006.

[6] D. A. Robinson, "A method of measuring eye movement using a scleral search coil in a magnetic field," *IEEE Trans. Biomed. Eng.*, vol. 10, no. 3, pp. 137–145, Oct. 1963.

[7] E. L. Bronaugh, "Helmholtz coils for calibration of probes and sensors: limits of magnetic field accuracy and uniformity," in *Proc. IEEE Int. Symp. Electromagn. Compat.*, Aug. 1995, pp. 72–76.

[8] N. Tziony, M. Itzkovich, and N. Moriya "Electrical circuit for crosstalk reduction," U.S. Patent 6 711 215, Mar. 23, 2004.

[9] A. Matveyev, *Principles of Electrodynamics*. New York: Reinhold, 1966.

[10] M. A. Wolfe, *Numerical Methods for Unconstrained Optimization, An Introduction*. New York: Van Nostrand, 1978.

[11] K. V. Price, R. M. Storn, and J. P. Lampinen, *Differential Evolution—A Practical Approach to Global Optimization*. New York: Springer-Verlag, 2005.

[12] *IEEE Standard for Safety Levels with Respect to Human Exposure to Electromagnetic Fields, 0–3 kHz,* IEEE Standard C95.6™, 2002.

[13] Motchenbacher, *Low-Noise Electronic System Design*. New York: Wiley-Interscience, 1993.

Anton Plotkin received the B.Sc. degree in radio, radio-broadcasting, and television engineering from the Siberian State University of Telecommunications and Informatics, Novosibirsk, Russia, in 1999 and the M.Sc. degree (*summa cum laude*) in electrical engineering from the Department of Electric and Computer Engineering, Ben-Gurion University of the Negev, Beer-Sheva, Israel, in 2004, where he is working toward the Ph.D. degree, since 2004.

Since 2004, he has been a Teaching Assistant with the Department of Electric and Computer Engineering, Ben-Gurion University of the Negev. Since 2008, he has been an Electronics Engineer with the Department of Neurobiology, Weizmann Institute of Sciences, Rehovot, Israel. His current research interests include magnetic tracking systems, magnetic sensors, and instrumentation for brain research and rehabilitation.

Oren Shafrir received the B.Sc. degree in electrical engineering and computers, in 2004, and the M.Sc. degree in electrical engineering, in 2009, both from the Ben-Gurion University of the Negev, Beer-Sheva, Israel.

His current interests include magnetic tracking systems for human computer interface, and very large scale integration design and verification.

Eugene Paperno received the B.Sc. and M.Sc. degrees in electrical engineering from the Minsk Institute of Radio Engineering, Minsk, Republic of Belarus, in 1983, and the Ph.D. degree (*summa cum laude*) from the Ben-Gurion University of the Negev, Beer-Sheva, Israel, in 1997.

From 1983 to 1991, he was with the Institute of Electronics, Belorussian Academy of Sciences, Minsk. From 1997 to 1999, he was a Japan Society for the Promotion of Science Postdoctoral Fellow with Kyushu University, Fukoka, Japan. Since 1999, he has been with the Department of Electrical and Computer Engineering, Ben-Gurion University of the Negev, where he was a Teaching Assistant from 1992 to 1997. His current interests include magnetic tracking systems for human computer interface and virtual reality systems.

Daniel M. Kaplan received the M.D. degree from Ben-Gurion University, Beer-Sheva, Israel, in 1992, and the M.H.A. degree in health administration, in 2006.

From 1992 to 1998, he was engaged in residency training with the Department of Otolaryngology-Head and Neck Surgery, Soroka University Medical Center, Beer-Sheva. From 1999 to 2001, he was a Clinical Fellow in otology and neurotology with the University of Toronto Hospitals, Toronto, Canada. Since 2001, he is a Staff Otolaryngologist with the Soroka University Medical Center, where he is currently a Senior Lecturer with the Ben-Gurion University and a Vice-acting Chief. His current interests include cochlear implant surgery for the deaf and testing of the vestibular system.